Available online at www.sciencedirect.com

ScienceDirect

Procedia Materials Science 5 (2014) 212 – 221

Procedia Materials Science

www.elsevier.com/locate/procedia

International Conference on Advances in Manufacturing and Materials Engineering, AMME 2014

Estimation of Crystallite Size, Lattice Strain and Dislocation Density of Nanocrystalline Carbonate Substituted Hydroxyapatite by X-ray Peak Variance Analysis

K. Venkateswarlu[a,b,*], M. Sandhyarani[a], T.A. Nellaippan[a], N. Rameshbabu[a]

[a]*Department of Metallurgical and Materials Engineering, National Institute of Technology, Tiruchirappalli 620015, Tamilnadu, India*

[b]*Department of Humanities and Sciences, Turbomachinery Institute of Technology and Sciences, Patancheru,Hyderabad-502319,Andhra Pradesh, India*

Abstract

X-ray peakprofile analysis by variance method is employed to evaluate the micro structural parameters namely crystallite size, mean squared lattice strain, root mean squared lattice strain and dislocation density of hydroxyapatite (HA) and carbonate substituted [3 wt% (3CHA) and 6 wt% (6CHA)] hydroxyapatite nanoparticles prepared by microwave synthesis technique. The calculated average crystallite sizes of HA, 3CHA and 6CHA by variance method are correlated with the values obtained from Scherer's and transmission electron microscopy (TEM) results. It is found that the results of the average crystallite size measured by variance analysis method are in good agreement with TEM results. The calculated micro structural parameters are also correlated with the *in-vitro* dissolution study results. It is found that variance method of X-ray peak profile analysis is more appropriate to quantify the micro structural parameters of nanostructured hydroxyapatite based nanoparticles.

Selection and peer-review under responsibility of Organizing Committee of AMME 2014

* Corresponding author. Tel.: +0-431-250-3471; fax: +0-431-250-0133.

E-mail address: kotharu.venkat@gmail.com

Selection and peer-review under responsibility of Organizing Committee of AMME 2014
doi:10.1016/j.mspro.2014.07.260

*Keywords:*Hydroxyapatite; Carbonate; Nanosize; Dissolution; XRD; TEM.

1. Introduction

Hydroxyapatite [HA, $Ca_{10}(PO_4)_6(OH)_2$] has been extensively used as a biomaterial in bone grafting, bone tissue engineering, and bone drug delivery due to its excellent properties of biocompatibility, bioactivity, osteoconductivity, non-toxicity, non inflammatoriness and non-immunogenicity. Although HA is considered as a good bone substitute, it is the least soluble and the most stable material among the calcium phosphates, which is an undesirable characteristic because it may impede the rate of bone regeneration upon implantation. It is always desirable that a bone substitute should be bioresorbable to some extent so that it can be replaced with the regenerated bone over a period of time. The resorbability of HA can be improved with the help of some ionic doping agents or by reducing its grain size to the nano level (Murugan and Ramakrishna, 2003). It was shown that the substitution of CO_3^{2-} into the apatite structure improves the resorbability of HA. The carbonate ions, which can occupy about 3-8 wt% of the calcified tissues, can be substituted either for the phosphate ion (B-type substitution) or for the hydroxyl ion (A-type substitution) or for both the ions (AB-type substitution) in the apatite lattice. The B-type substitution of CO_3^{2-} leads to a decrease of a-axis and an increase of the c-axis of the HA lattice (LeGeros, 1965; LeGeros et al., 1967). The presence of B-type CO_3^{2-} in the apatite lattice was shown to cause an increase in solubility both *in-vitro* and *in-vivo* tests (Krajewski et al., 2005). Hence, among the variety of HA-based ceramics, carbonated HA (CHA) appears to be an excellent material for bioresorbable bone substitutes (Suchaneka et al., 2002)

Nanocrystalline HA-based ceramics such as nano CHA is expected to have homogeneous resorption and better bioactivity than coarser crystals (Webster et al., 2001). The properties and the performance of HA based bioceramics can be improved by changing powder particle size and shape, their distribution and agglomeration (Best and Bonfield, 1994). Apart from this, it was recently reported that nanosized CHA crystals with low crystallinity could be successfully applied to fabricate CHA/collagen biodegradable composites and when these composite materials were implanted in rabbits, they underwent resorption and promoted new bone formation (Du et al., 1998). Therefore, synthesis of CHA powders with desired properties such as nano size, low crystallinity, controlled morphology and chemical composition is of great importance.

Many researchers [LeGeros et al., 1967; Lafon et al., 2003; Pan and Darvel, 2010] have reported various methods of preparation of carbonated HA and studied the effect of carbonate substitution on lattice parameters, morphology, thermal decomposition and solubility of HA. In addition a few researchers (Krajewski et al., 2005) have studied the various types (A, B and AB) of CO_3^{2-} substitution and the various quantification methods of CO_3^{2-} in HA lattice. But a certain gap exists in the literature in estimating and correlating the micro structural parameters such as the accurate crystallite size, the mean squared lattice strain, the root mean squared lattice strain and the dislocation density to the structural and the dissolution properties of CHA, which might provide the information for better understanding of the differences in dissolution properties of CHA compared to the HA.

For better correlation of the nanoscale material properties to their above mentioned micro structural parameters thereby achieving proper understanding and prediction, their size is required to be calculated as accurately as possible. So far, Scherrer method is a well known method to calculate the crystallite size based on the broadening of the X-ray diffraction peaks from the powder diffraction data. However, Scherrer method underestimates the crystallite size because of not considering the instrumental and strain contribution to the X-ray diffraction peak broadening. Hence X-ray diffraction peak profile analysis has been widely used to calculate the crystallite size more accurately by considering all the other important factors such as instrumental and strain contribution to the X-ray diffraction peak broadening. Apart from these, the various analytical methods such as the whole diffraction pattern fitting methods are also being used to estimate the crystallite size and the lattice strain present in the material from X-ray peak broadening (Warren and Averbach, 1950). However, fitting the complete powder diffraction data accurately is complicated and hence it attracts many indirect methods such as Williamson-Hall (W-H) method and Warren- Averbach (W-A) analysis for estimating the lattice strain and crystallite size [Warren et al., 1951;

Williamson and Hall, 1953). In W-A analysis the intensity of the diffracted X-ray beam is calculated in Fourier space and this intensity is considered as a value given by the convolution of size and strain broadening (Warren, 1969). Whereas W-H analysis is a simplified method which clearly differentiates between size induced and strain induced peak broadening by considering the peak width as a function of 2θ (Suryanarayana and Norton, 1998). In addition to these, the *variance method* of X-ray diffraction peak profile analysis is a superior method of calculating the crystallite size and the lattice strain present in the nanosized materials based on the angular range over which the intensity of the diffraction peak is measured.

The objective of this work is to estimate and compare the microstructural parameters namely crystallite size, mean squared and root mean squared lattice strain and dislocation density of HA and CHA by using *variance method* of X-ray diffraction peak profile analysis, thereby correlating the calculated microstructural parameter values to the differences in the dissolution properties of HA and CHA. For this purpose 3 wt% and 6 wt%, which falls in the occupancy range (3-8 wt %) of natural biological apatite, carbonated substituted HA particles are prepared by microwave synthesis method and are analyzed.

2. Experimental

2.1 Synthesis of HA, 3CHA and 6CHA nanoparticles

HA and CHA (3CHA and 6CHA) nanoparticles were prepared under identical processing conditions using microwave synthesis method. Analytical grade calcium hydroxide [$Ca(OH)_2$, E. Merck, Germany], di-ammonium hydrogen phosphate [DAP, $(NH_4)_2HPO_4$, E. Merck, Germany] and calcium carbonate [$CaCO_3$, E. Merck, Germany] were used as precursor materials for the preparation of HA and CHA nanoparticles. The amount of the reactants was calculated based on the Ca/P and Ca/(P+C) molar ratio of 10/6 respectively for HA and CHA. For the preparation of HA, the 0.3 M DAP solutions in a glass beaker is added to the 0.3 M calcium hydroxide aqueous suspension in 1000 ml glass beaker in 5 min under vigorous stirring conditions. This 1000 ml glass beaker containing the precursor mixture with pH of about 11 (Orion 3 star, Thermo electron, USA) is immediately subjected to the microwave irradiation for an optimized time of 30 min (Rameshbabu et al., 2010) in a domestic microwave oven (Samsung India, 2.45 GHz, 850 W power). For CHAs preparation, the calcium carbonate aqueous suspension with 0.25M concentration was prepared separately and added to the 0.3 M calcium hydroxide aqueous suspension in parallel to the DAP solution under vigorous stirring conditions for 5 min. The mixing, crystallization and aging of HA and CHA's occur under the microwave irradiation in a shorter period. The products obtained after filtration were dried at 85 °C for 24 h and the cakes obtained after drying were powdered separately with agate mortar and pestle.

2.2. Characterization

The X-ray diffraction is carried out for these as-synthesized powder particles by using a Rigaku Ultima III X-ray diffractometer with Cu $K_{\alpha 1}$ radiation (λ = 1.54056 Å) over the 2θ range of 20–60°, using a step size of 0.02° and step time of 4 s. The preferred high intensity peaks (002, 310, 222, 213 and 004) corresponding to comparatively higher diffraction angle were chosen to estimate the micro structural parameters by variance analysis of X-ray diffraction peak profiles. The functional groups present in as-prepared HA and CHA were ascertained by FTIR (Perkin Elmer, Spectrum One, USA) over the region 450–4000 cm^{-1} in pellet form for the powder samples of 1 mg mixed with spectroscopic grade KBr (Merck) of 200 mg. Spectra were recorded at 4 cm^{-1} resolution, averaging 80 scans. The size and the morphology of HA and CHA powder particles were analyzed by transmission electron microscope (TEM, Philips, CM12 STEM, Netherlands). For TEM analysis, the powder samples were ultrasonically dispersed in ethanol to form dilute suspensions, and then a few drops were deposited on the carbon-coated copper grids.

2.3 In-vitro dissolution study of HA and CHA

The *in-vitro* dissolution studies of HA, 3CHA and 6CHA were carried out under simulated osteoclastic resorption conditions at a pH of about 4.5 (Rameshbabu and Prasad Rao, 2009) in order to simulate general remodelling of the skeletal system. Compacts were prepared by uniaxially pressing 300 mg of powder at 300 MPa in a 10 mm diameter stainless steel die. The initial weights of the compacted samples were noted. The compacted samples were immersed into 4.5 pH medium (prepared by adding diluted nitric acid to double distilled water) of 100 ml each at temperature 37 °C. The pH was checked and adjusted at regular intervals (3 h). If the pH was increased due to neutralization of the basic calcium phosphate, 0.001 N HNO_3 was added in order to maintain an average pH of 4.5. The samples were taken out after 72 h and weighed after drying.

3. Results and discussion

3.1 XRD and FTIR analysis of HA and CHA nanoparticles

The XRD spectra of as-synthesized HA, 3CHA and 6CHA samples are shown in Fig. 1(a), (b) and (c) respectively.

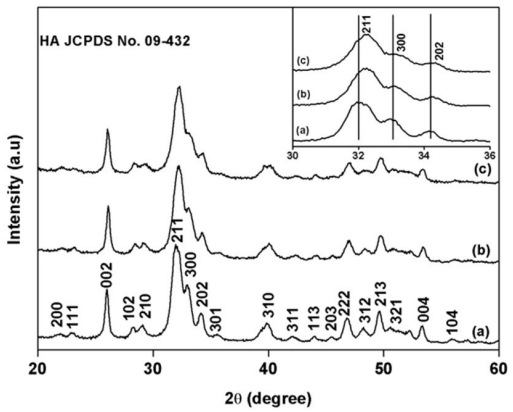

Fig. 1. XRD patterns of as-synthesized nanocrystalline HA (a), 3CHA (b) and 6CHA (c)

The XRD spectra of HA, 3CHA and 6CHA are similar and exhibit several diffraction peaks which are well matched with the diffraction peaks of the standard JCPDS (09-432) pattern of hydroxyapatite and can be assigned to hexagonal crystal structure with space group $P6_3/m$. In addition, the diffraction peaks are markedly broader suggesting that the prepared powder particles are in nanosize. As compared to the X-ray diffraction peaks of HA particles [Fig. 1(a)], the diffraction peaks of 3CHA and 6CHA particles [Fig. 1(b) and (c)] are progressively broader indicating that the crystallinity of HA decreases successively with an increase of carbonate substitution. The calculated average full width at half maximum of the diffraction peaks taken for the variance analysis are 0.5232, 0.5924 and 0.6523° respectively for HA, 3CHA and 6CHA. The decrease of HA crystallinity with an increase of carbonate substitution in to HA lattice is also evident from the progressively reduced intensity of the hollow between 300 and 112 (merged with 211) diffraction peaks. This confirms that the substitution of carbonate ions in to the HA lattice could degrade the crystallinity of HA. To confirm the substitution of carbonate in to HA lattice, the XRD patterns around the main peak (2θ = 30-36°) of HA, 3CHA and 6CHA [(a), (b) and (c) respectively] samples were expanded and are shown in the inset graph of Fig. 1. The shift of 211, 300 and 202 diffraction peaks in both 3CHA and 6CHA towards higher angle compared to HA clearly suggests the substitution of carbonate in HA lattice. The shift of the diffraction peaks towards higher or lower diffraction angles is in accordance with the Bragg's diffraction law [$2d_{hkl} \sin\theta_{hkl} = n\lambda$] and depends on the smaller or larger size of the substituted species (Cullity, 1978). The shift of 211, 300 and 202 diffraction peaks [Fig. 1 inset graph] in both 3CHA and 6CHA towards higher angle compared to HA is due to the substitution of smaller carbonate ions to larger phosphate ions in HA lattice. The

decreasing trend of a-axis with increasing carbonate content is due to the replacement of larger phosphate ion with smaller carbonate ion which is also responsible for the shift of the entire diffraction pattern towards a higher diffraction angle as shown in the inset graph of Fig. 1. The XRD results thus indicate the formation of B -type carbonated HA. The absence of impurities and the B-type substitution of CO_3^{2-} in the HA lattice are also proved by FTIR analysis.

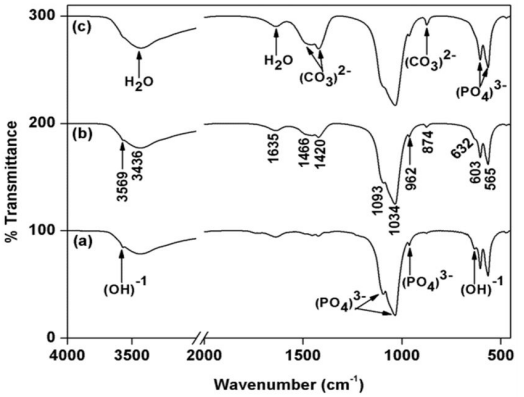

Fig. 2. FTIR spectra of as-synthesized nanocrystalline HA (a), 3CHA (b) and 6CHA (c)

The FTIR spectra of HA, 3CHA and 6CHA samples are shown in Fig. 2 (a), (b) and (c) respectively. In the middle infrared region, the HA spectrum [Fig. 2 (a)] displays all the peaks pertaining to hydroxyl (OH^-), water (H-O-H) and phosphate (PO_4^{3-}) functional groups. The spectra of 3CHA [Fig. 2 (b)] and 6CHA [Fig. 2 (c)] show the characteristic absorption bands of the HA in addition to CO_3^{2-} bands indicating the formation of CHA. The characteristic bands were exhibited in all the spectra at their respective band positions: 900–1200 cm^{-1} for phosphate bending and stretching, 603 cm^{-1} for phosphate bending. The increased broadening of the phosphate characteristic bands at 1034 and 1093 cm^{-1} for 3CHA and 6CHA compared to HA is due to reduced crystallinity and small dimensional effects of 3CHA and 6CHA particles. The decrease in crystallinity with an increase of carbonate substitution is also evident from the successive decrease in intensity of the characteristic bands at 632 cm^{-1} and 3569 cm^{-1} for librational & stretching modes of hydroxyl vibrations of 3CHA and 6CHA compared to that of HA. Hence it is confirmed that the increasing amounts of carbonate substitution make the HA structure more amorphous which is in good agreement with the result reported by other researchers (Krajewski et al., 2005). The absorption bands at 874, 1420 and 1466 cm^{-1} for 3CHA and 6CHA correspond to the CO_3^{2-} substitution for B-site (forPO_4^{3-} groups) in HA. The increase in the intensity of the absorption bands at 874, 1420 and 1466 cm^{-1} for 6CHA compared to 3CHA corresponds to the increased CO_3^{2-} substitution for B-site. The less intensity absorption bands at 874, 1420 and 1466 cm^{-1} are also observed in HA that are corresponding to the presence of carbonate ions, which may come from a reaction between the carbon dioxide in air and the high pH precursor solution (Kumta et al., 2005). However, the increase in intensity of these absorption bands for 3CHA and 6CHA confirms the substitution of carbonate in HA lattice. Thus both the XRD and FTIR results confirm the B-type CO_3^{2-} substitution in HA. As it was reported that B-type CHA is the most abundant species in human bone (Landi et al., 2003), the prepared CHA particles are chemically and structurally analogous to the biological apatite in human bone.

3.2 Determination of crystallite size of HA and CHA by Scherrer analysis

Generally, the X-ray diffraction peak broadening is due to the instrumental broadening, broadening due to the crystallite size and the lattice strain present in the material. The contributions of each of these effects are convoluted causing an overall broadening of the diffraction peaks. Before estimating the crystallite size and the lattice strain, it is necessary to correct the instrumental effect. The instrumental corrected broadening β_{hkl}corresponding to the diffraction peaks of HA and CHA was estimated using the equation:

$$\beta_{hkl} = \left(\beta_{hkl}\right)^2_{measured} - \left(\beta\right)^2_{instrumental}{}^{1/2} \quad (1)$$

It is well known that the Scherer's formula provides only the lower bound to the crystallite size. Here the crystallite size value is calculated by using Scherer's formula to compare with the values obtained from the variance and TEM analysis results.The crystallite sizes D_v of HA, 3CHA and 6CHA were estimated from the Scherer's equation as given below:

$$D_v = \frac{k\lambda}{\beta_{hkl}\cos\theta_{hkl}} \quad (2)$$

Where,D_v is the volume weighted crystallite size (nm); k is the shape factor (k = 0.9); λ is the wavelength of the X-rays (λ = 0.154056 nm for Cu $K\alpha_1$ radiation); θ_{hkl} is Bragg diffraction angle (°) and β_{hkl} is the broadening of the *hkl* diffraction peak measured at half of its maximum intensity (in radians). The volume weighted crystallite size D_v measured by using Scherrer's formula were found to be 25, 22 and 20 nm for HA, 3CHA and 6CHA respectively.

3.3 Determination of crystallite size and lattice strain by variance analysis

If a crystal is broken into smaller incoherently diffracting domains by dislocation arrays (small angle boundaries), stacking faults, twins, large angle boundaries (grains), or any other extended imperfections, then domain-size broadening occurs. Any lattice imperfection will cause diffraction line broadening. Therefore, dislocations, vacancies, interstitials, substitutional, and similar defects lead to lattice strain (Waje et al., 2010). Variance analysis is the most frequently used analytical technique for separating the domain size and the lattice strain broadening to calculate the crystallite size and the lattice strain more accurately. The applicability of the variance or mean square breadth to the analysis of the line broadening of the X-ray diffraction peaks was clearly demonstrated by Wilson. If the line broadening is due both to the crystallite size and the lattice strain, then the variance in 2θ coordinates also called mean square breadth (Aqua, 1966) is given by

$$W(2\theta) = \beta^2_{hkl} = \frac{\lambda\Delta(2\theta)}{2\pi^2 P\cos\theta} + 4\tan^2\theta\langle\varepsilon^2\rangle \quad (3)$$

Where Δ (2θ) is the angular range over which the intensity of the diffraction peak is measured (radian), P is the apparent crystallite size (nm) and $\langle\varepsilon^2\rangle$ is the mean square strain. The effective or real crystallite size, P_e, is defined by the ratio P/K, where K is the crystallite shape factor. The crystallite size and the strain contributions to the true variance, obtained after instrumental profile correction, are separated by plotting a graph by taking 4 $\tan^2\theta$ along x-axis and β^2_{hkl} along y-axis. The crystallite size (nm) and the lattice strain were extracted respectively from the intercept and the slope of the linear fit made to the plot drawn by taking 4 $\tan^2\theta$ along x-axis and β^2_{hkl} along y-axis.

The dislocation density (ρ) is defined as the length of the dislocation lines per unit volume of the crystal (Warren and Warekois, 1955). Williamson and Smallman (1956) suggested a method of calculating the dislocation density using the expression:

$$\rho = \left[\frac{\sqrt{12}\langle\varepsilon^2\rangle^{1/2}}{Pd}\right] \quad (4)$$

Where $\langle\varepsilon^2\rangle^{1/2}$ is the root mean square (rms) strain and d is the interplanar spacing.

The variance plots drawn by taking 4 $\tan^2\theta$ along x-axis and β^2_{hkl} along y-axis are shown in Fig. 3 (a), (b) and (c) for HA, 3CHA and 6CHA respectively. Assuming that the strain present in the material is uniform, the crystallite size and the lattice strain values are extracted respectively from the intercept and the slope of the linear fit made to plot drawn by taking 4 $\tan^2\theta$ along x-axis and β^2_{hkl} along y-axis.

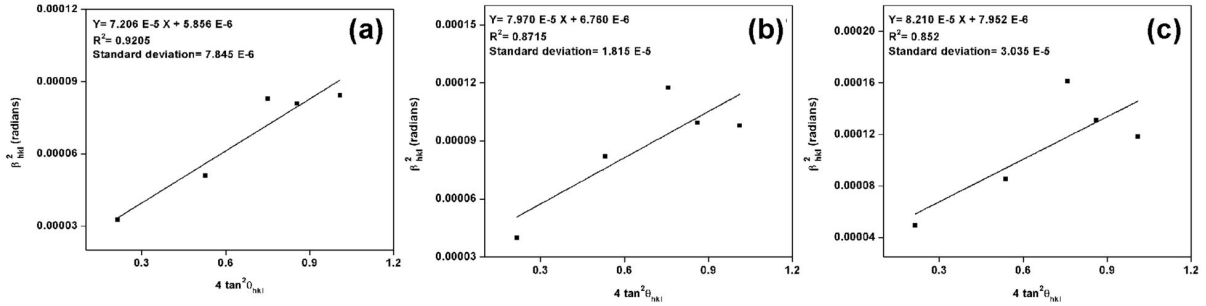

Fig. 3. Variance analysis plots of as-synthesized nanocrystalline HA (a), 3CHA (b) and 6CHA (c)

The estimated values of crystallite size, the lattice strain and the dislocation density for HA, 3CHA and 6CHA are shown in Table 1. There is a significant difference between the average crystallite size calculated by the Scherrer method and that obtained from TEM image analysis, whereas, a good correlation is observed between the average crystallite size calculated by variance analysis and that obtained by TEM analysis. This observation suggests the importance of deconvoluting the instrumental and the lattice strain broadening while calculating the crystallite size of especially nanocrystalline materials from X-ray peak broadeningwhich is also reported by the authors in previous study (Venkateswarlu et al., 2010). It is also observed from Table 1 that the crystallite size is decreased with the increase of carbonate substitution in HA lattice. This is due to the successive degradation of crystalline HA lattice with the progressive incorporation of smaller planar carbonate ions in to the lattice sites of larger tetragonal phosphate ions of HA which are also confirmed by the broadening effect of XRD and FTIR spectra. The lattice strain is observed to be increased with the increase of carbonate content. The trend of increasing lattice strain with an increase of carbonate substitution is due to the increase of dislocations, micro stresses, long range internal stresses, grain boundaries, coherency strains and crystallite smallness which are the main contributors of lattice strain (Ungar, 2004). This can be further justified by the increased dislocation density with an increase of carbonate content in HA lattice as shown in Table 1.

Table 1 The estimated microstructural parameters of as-synthesized nanocrystalline HA and CHA

Sample	Scherrer analysis	Variance analysis			TEM analysis	Dislocation density
	D_v (nm)	P_e (nm)	$<\varepsilon^2> \times 10^{-5}$ (no unit)	$\varepsilon_{rms} \times 10^{-3}$ (no unit)	D_v (nm)	$\rho \times 10^{14}$ (line/m^2)
HA	25	40	7.20	8.48	44±4	5.35
3CHA	22	36	7.97	8.92	39±5	6.28
6CHA	20	33	8.21	9.06	35±3	7.15

The increase of micro stresses with an increase of carbonate content can be understood in terms of the charge balancing mechanism: Generally, when a carbonate ion (CO_3^{2-}) substitutes for a OH^- (A-type) or a PO_4^{3-} (B-type) in HA lattice, the local charge compensation takes place by OH vacancy for A-type and by a combination of OH and Ca vacancies for B-type substitution. For AB-type carbonate substitution, the local charge compensation takes place by a combination of two Ca and one OH vacancy per three B-site carbonate substitutions (Astala and Stott, 2005). As the prepared CHA particles are of B-type carbonate substituted, the local charge balance takes place by a combination of OH and Ca vacancies. Thus the charge compensating cationic and anionic vacancies, the chemical heterogeneity and the difference in ionic radii of hydroxyl, carbonate and phosphate ions can be attributed to the increase of stress fields in HA lattice which intern are responsible for the increased lattice strain with an increase of carbonate substitution. The increased lattice strain, which is due to increase in dislocations, micro stresses, grain boundaries, coherency strains and crystallite smallness, is reflected by the increased broadening of the diffraction peaks with the increase of carbonate substitution (Fig. 1), whereas the successive increase in peak shift of the diffraction peaks (as shown in inset graph of Fig. 1) correspond mainly to the increase in stacking faults and twinning (Ungar, 2004). Thus from the increase in peak broadening and peak shift, it is concluded that the HA structure becomes more defective and will be thermodynamically in high energy state with the increase of carbonate

substitution. In the present study the root mean square error (RMSE) or standard deviation (SD) of experimental data points from the ideal linear fit for HA [Fig. 3 (a)], 3CHA [Fig. 3 (b)] and 6CHA [Fig. 3 (c)] are respectively given by 7.84×10^{-6}, 1.81×10^{-5} and 3.03×10^{-5}. Though the data points seem to be visually scattered from their respective variance plots, the standard deviation data show that the scatter from the linear fit is about the order of 10^{-6} in case of HA, and of the order of 10^{-5} for 3CHA and 6CHA. This much less significant SD from the linear fit of the three samples supports that the assumption, of uniform strain in all crystallographic directions for the three samples, made in the present analysis is acceptable in a reasonable approximation. This is further justified from the R^2 values, which confirm how well the experimental data could be approximated by linear relationship, of the linear fit of the variance plots. However, the scattering of the experimental data points away from the linear fit is very much less significant in HA compared to 3CHA and 6CHA. This confirms that the assumption of the uniform strain holds good more in HA compared to that of 3CHA and 6CHA. This successive deviation from the uniformity of lattice strain with an increase of carbonate substitution might be due to the increased modifications introduced by the carbonate substitution derived stress fields.However, the data points are close to the linear fit in all the three plots and hence the estimated crystallite size for HA, 3CHA and 6CHA are in good agreement with the TEM results as discussed in section 3.5.

3.4 Dissolution study of HA and CHA particles

The relative weights of HA, 3CHA and 6CHA after 72 h in simulated osteoclastic resorption condition are shown in Fig. 4. The chemical stability of the HAs at osteoclastic resorption condition, decreased with an increase in carbonate substitution, as evidenced by the increasing rate of dissolution from HA to 6CHA. These *in-vitro* results suggest that the carbonate substitutions in HA offer the ability to prepare HAs with different degrees of solubility.

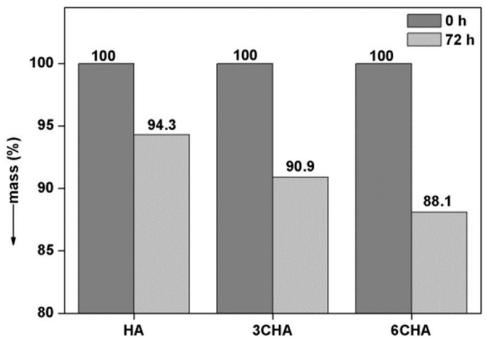

Fig. 4. Solubility of HA, 3CHA and 6CHA in simulated osteoclastic resorption condition of 4.5 pH

The nanocrystalline 6CHA possessing slightly higher solubility than the nanocrystalline 3CHA or HA under the conditions of osteoclastic resorption may be a preferred material for bone applications, where higher solubility is required to participate in the general remodelling of the skeletal system. The nanocrystalline HAs with different carbonate contents (CHAs), having different solubility behaviour, would enable the surgeons to choose the appropriate material for the needs of specific application. The higher solubility of 6CHA can be attributed to its higher dislocation density compared to that of 3CHA and HA. Higher the dislocation density more is the dissolution rate. This is due to the fact that dislocations are thermodynamically unstable, having an associated localized energy which results in an increase in free energy and a reduction in the activation energy for dissolution at points where they emerge on the crystal face. Hence it may be speculated that a crystal, intern material, with a higher dislocation density should have a higher thermodynamic activity which may result in a greater overall dissolution rate. Thus the greater chemical potential at the dislocation core and the localized energy of dislocations in 6CHA are responsible for the enhanced dissolution compared to that of 3CHA and HA. A brief mechanism of the dissolution of the prepared powder particles can be given as follows. The dislocations which are linear defects at an atomic scale are preferential sites for dissolution. When the powder particles are kept in the test medium, firstly an etch pit with hexagonal symmetry is formed at the dislocation site (where the dislocation line points through the surface) and the

pit extends in to the crystal in a direction perpendicular to the basal plane (0001) which results in successive dissolution. A detailed mechanism of dissolution of single crystal hydroxyapatite in citric and lactic acids was reported by other researchers (Jongebloed et al., 1974). Hence, it can be concluded that the 6CHA with a higher dislocation density is more likely to be attacked by the acids on the surface, compared to that of 3CHA and HA. This results in the higher dissolution rate for 6CHA compared to that of 3CHA and HA.

3.5 TEM analysis of HA and CHA particles

The bright field transmission electron microscopic images of HA, 3CHA and 6CHA nanoparticles in as-synthesized condition are shown in Fig. 5 (a), (b) and (c), respectively. The HA particles are of rod-like shaped morphology and are a bit longer with more regular and clear contour. In addition, the HA particles showed comparatively less tendency to agglomerate as shown in Fig. 5 (a). In comparison to the HA particles, 3CHA particles look like with near-rod like or needle like shaped morphology and with a similar tendency to agglomerate. On the other hand, 6CHA particles look like with ellipsoid like shaped morphology and with a comparatively more tendency to agglomerate. This is due to the fact that as the carbonate content in HA lattice increases, the apatite structure becomes more amorphous and results in an increased agglomeration. The sizes of HA and CHA nanoparticles are estimated from TEM images by image analysis done with a freely available IMAGE J software. The HA particles exhibited a length of about 67 nm and a width of about 21 nm corresponding to an aspect ratio of about 3.19. On the other hand the 3CHA particles exhibited a length of about 59 nm and a width of about 19 nm corresponding to an aspect ratio of about 3.10. Similarly, 6CHA particles exhibited a length of about 53 nm and a width of about 17 nm corresponding to an aspect ratio of about 3.11. However, to correlate the results obtained from various analyses, the sizes of HA and CHA obtained from TEM analysis were expressed as (length + width)/2 and are given as 44 ± 4, 39 ± 5 and 35± 3 nm (mean ± SD) for HA, 3CHA and 6CHA respectively. From the above results of TEM analysis it can be concluded that the particle morphology is modified from rod-like shape of HA particles to extended ellipsoid like shape morphology of the 6CHA particles with increase of carbonate content in HA lattice. Similar trend of modification in the morphology of crystalline HA particles fromrod like shape to spherical shape with increase of carbonate content were also observed by other researchers (Liao et al., 2007).

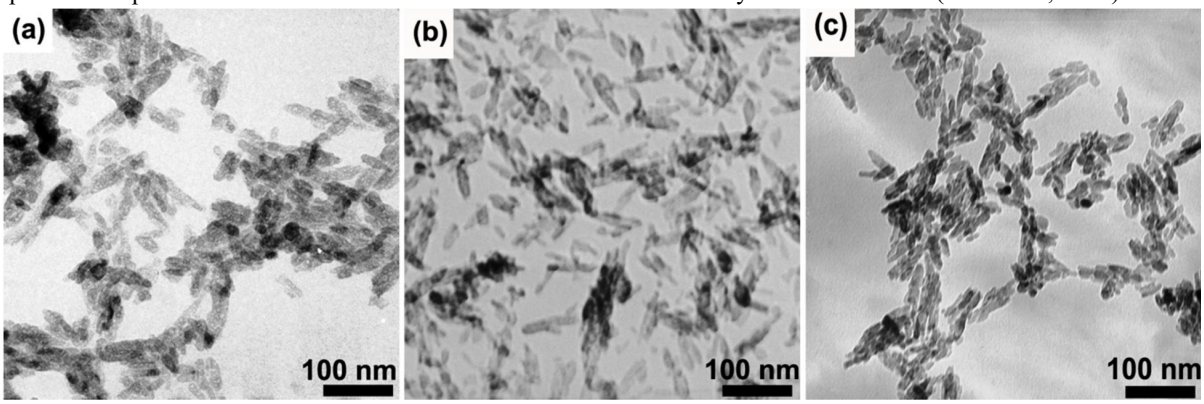

Fig. 5. TEM micrographs of as-synthesized nanocrystalline HA (a), 3CHA (b) and 6CHA (c)

4. Conclusions

Nanocrystalline HA and CHA particles were successfully synthesized by microwave method under identical processing conditions. There is a significant difference between obtained crystallite size value by the Scherrer analysis and the TEM analysis for HA and CHA particles. There is a good agreement between the crystallite size values obtained by variance analysis and that obtained by TEM analysis for HA and CHA powder particles. Hence, variance analysis results are more accurate for the estimation of crystallite size, when compared to Scherrer analysis. Therefore it is suggested that the contribution from the instrumental effects and the lattice strain effect to the X-ray

peak broadening need to be considered while calculating the crystallite size value of nanomaterials. The variance analysis can also be applied to estimate more accurately the other microstructural parameter such as lattice strain and thereby dislocation density present in the material under study. The incorporation of CO_3^{2-} in the crystal lattice of HA results in lower crystallinity, crystallite size, the higher lattice strain and the higher dislocation density of HA which in turn are responsible for the improved solubility of CHA under the performed test conditions. The substitution of carbonate in HA lattice results in an increase in dislocation density, which in turn increases the active sites for dissolution by the acid medium.

References

Aqua, E.D., 1966. The separation of particle size and strain by the method of the variance, Acta Crystallographica 20, 560-563.

Astala, R., Stott, M.J., 2005. First principles investigation of mineral component of bone: CO3 substitutions in hydroxyapatite, Chemistry of Materials 17, 4125-4133.

Best, S., Bonfield, W., 1994. Processing behaviour of hydroxyapatite powders with contrasting morphology, Journal of Materials Science: Materials in Medicine 5, 516-521.

Cullity, B.D., 1978. Elements of X-ray diffraction, Addison-Wesley Publishing Company, Inc., London.

Du, C., Cui, F.Z., Feng, Q.L., Zhu, X.D., Groot, K.D., 1998. Tissue response to nano-hydroxyapatite/collagen composite implants in marrow cavity, Journal of Biomedical. Materials Research 42, 540-548.

Jongebloed, W.L., Vandenberg, P.J., Arends, J., 1974. The dissolution of single crystals of hydroxyapatite in citric and lactic acids, Calcified tissue research 15, 1-9.

Krajewski, A., Mazzocchi, M., Buldini, P.L., Ravaglioli, A., Tinti, A., Taddei, P., Fagnano, C., 2005. Synthesis of carbonated hydroxyapatite: efficiency of the substitution and critical evaluation of analytical methods, Journal of Molecular Structure744, 221-228.

Kumta, P.N., Sfeir, C., Lee, D.H., Olton, D., Choi, D., 2005. Nanostructured calcium phosphates for biomedical applications: novel synthesis and characterization, Acta Biomaterialia 1, 65-83.

Lafon, J.P., Champion, E., Assollant, D.B., Gibert, R., Danna, A.M., 2003. Thermal decomposition of carbonated calcium phosphate apatites, Journal of thermal analysis and calorimetry 72, 1127-1134.

Landi, E., Celotti, G., Logroscino, G., Tampieri, A., 2003. Carbonated hydroxyapatite as a bone substitute, Journal of European Ceramic Society 23, 2931-2937.

LeGeros, R.Z., 1965. Effect of carbonate on the lattice parameters of apatite, Nature 206, 403-404.

LeGeros, R.Z., Trautz, O.R., LeGeros, J.P., Klein, E, Paul, S.W., 1967. Apatite crystallites: Effects of carbonate on morphology, Science 155, 1409-1411.

Liao, S., Watari, F., Xu, G., Ngiam, M., Ramakrishna, S., Chan, C.K., Morphological effects of variant carbonates in biomimetic hydroxyapatite, Materials Letters 61, 3624-3628.

Murugan. R., Ramakrishna, S., 2003. Effect of zirconia on the formation of calcium phosphate bioceramics under microwave irradiation, Materials Letters 58, 230-234.

Pan, H.B., Darvell, B.W., 2010. "Carbonate affect the solubility of hydroxyapatite, Crystal Growth and Design 10, 845-850.

Rameshbabu, N., Prasad Rao, K., 2009. Microwave synthesis, characterization and in-vitro evaluation of nanostructured biphasic calcium phosphates, Current Applied Physics 9, S29-S31.

Rameshbabu, N., Sampath Kumar, T.S., Prasad Rao, K., 2010. Influence of microwave power, irradiation time and polymeric additions on synthesis of nanocrystalline hydroxyapatite, Materials Research Innovations 14, 45-50.

Suchaneka, W.L., P. Shuka, Byrappaa, K., Rimana, R.E., TenHuisenb, K.S., Janas, V.F., 2002. Mechanochemical–hydrothermal synthesis of carbonated apatite powders at room temperature, Biomaterials 23, 699-710.

Suryanarayana, C., Norton, M.G., 1998. X-ray Diffraction: A Practical Approach, Plenum Press, New York.

Ungar, T., 2004. Microstructural parameters from X-ray diffraction peak broadening, Scripta Materillia 51, 777-781.

Venkateswarlu, K., Bose, A.C., Rameshbabu, N., 2010. X-ray peak broadening studies of nanocrystalline hydroxyapatite by Williamson–Hall analysis, Physica B: Condensed Matter 405, 4256-4261.

Waje, S.B., Hashim, M., Yusoff, W.D.W., Abbas, Z., 2010. X-ray diffraction studies on crystallite size evolution of $CoFe_2O_4$ nanoparticles prepared using mechanical alloying and sintering, Applied Surface Science 256, 3122-3127.

Warren, B.E., 1969. X-ray Diffraction, Dover Publications, New York.

Warren, B.E., Averbach, B.L., 1950. The Effect of Cold Work Distortion on X-Ray Patterns, Journal of Applied Physics 21, 595-599.

Warren, B.E., Averbach, B.L., Roberts, B.W., 1951. Atomic Size Effect in the X-Ray scattering by Alloys, Journal of Applied Physics 22, 1493-1496.

Warren, B.E., Warekois, E.P., 1955. Stacking Faults in Cold Worked Alpha-Brass, Acta Metallurgica 3, 473-479.

Webster, T.J., Ergun, C., Doremus, R.H., Siegel, R.W., Bizios, R., 2001. Enhanced osteoclast-like cell functions on nanophase ceramics, Biomaterials 22, 1327-1333.

Williamson, G.K., Hall, W.H., 1953. X-ray line broadening from filed aluminium and wolfram, Acta Metallurica 1, 22-31.

Williamson, G.K., Smallman, R.E., 1956. Dislocation densities in some annealed and cold-worked metals from measurements on the X-ray debye-scherrer spectrum, Philosophical Magazine 1, 34-46.